Depth profile of the ferromagnetic order in a YBa$_2$Cu$_3$O$_7$/La$_{2/3}$Ca$_{1/3}$MnO$_3$ superlattice on a LSAT substrate: A polarized neutron reflectometry study

M. A. Uribe-Laverde,[1,*] D. K. Satapathy,[1,†] I. Marozau,[1] V. K. Malik,[1] S. Das,[1] K. Sen,[1] J. Stahn,[2] A. Rühm,[3] J.-H. Kim,[4] T. Keller,[4] A. Devishvili,[5] B. P. Toperverg,[5] and C. Bernhard[1]

[1]*University of Fribourg, Department of Physics, and Fribourg Centre for Nanomaterials, Chemin du Musée 3, CH-1700 Fribourg, Switzerland*
[2]*Laboratory for Neutron Scattering, Paul Scherrer Institut, CH-5232 Villigen, Switzerland*
[3]*Max-Planck-Institut für Intelligente Systeme, Heisenbergstrasse 3, D-70569 Stuttgart, Germany*
[4]*Max-Planck-Institut für Festkörperforschung, Heisenbergstrasse 1, D-70569 Stuttgart, Germany*
[5]*Institute of Solid State Physics, Ruhr-Universität Bochum, D-44801 Bochum, Germany*

Using polarized neutron reflectometry (PNR) we have investigated a [YBa$_2$Cu$_3$O$_7$(10 nm)/La$_{2/3}$Ca$_{1/3}$MnO$_3$ (9 nm)]$_{10}$ (YBCO/LCMO) superlattice grown by pulsed laser deposition on a La$_{0.3}$Sr$_{0.7}$Al$_{0.65}$Ta$_{0.35}$O$_3$ (LSAT) substrate. Due to the high structural quality of the superlattice and the substrate, the specular reflectivity signal extends with a high signal-to-background ratio beyond the fourth-order superlattice Bragg peak. This allows us to obtain more detailed and reliable information about the magnetic depth profile than in previous PNR studies on similar superlattices that were partially impeded by problems related to the low-temperature structural transitions of the SrTiO$_3$ substrates. In agreement with the previous reports, our PNR data reveal a strong magnetic proximity effect showing that the depth profile of the magnetic potential differs significantly from the one of the nuclear potential that is given by the YBCO and LCMO layer thickness. We present fits of the PNR data using different simple blocklike models for which either a large ferromagnetic moment is induced on the YBCO side of the interfaces or the ferromagnetic order is suppressed on the LCMO side. We show that a good agreement with the PNR data and with the average magnetization as obtained from dc magnetization data can only be obtained with the latter model where a so-called depleted layer with a strongly suppressed ferromagnetic moment develops on the LCMO side of the interfaces. We also show that the PNR data are still compatible with the presence of a small, ferromagnetic Cu moment of 0.25 μ_B on the YBCO side that was previously identified with x-ray magnetic circular dichroism and x-ray resonant magnetic reflectometry measurements on the same superlattice [D. K. Satapathy *et al.*, [Phys. Rev. Lett. **108**, 197201 (2012)]. We discuss that the depleted layer thus should not be mistaken with a "dead" layer that is entirely nonmagnetic but rather may contain a canted antiferromagnetic or an oscillatory type of ordering of the Mn moments that is not detected with the PNR technique.

The interaction of the competing superconducting (SC) and ferromagnetic (FM) order parameters is a fascinating topic that has been extensively studied theoretically and experimentally.[1–3] In recent years significant progress has been made with thin-film heterostructures from conventional superconductors and elemental or alloy ferromagnets where effects such as domain wall superconductivity,[4] critical temperature oscillations with the thickness of the FM layer in SC/FM/SC junctions,[5] and a long-range proximity effect of a spin-triplet SC state through composite FM layers with a noncollinear magnetic order[6] were predicted theoretically and confirmed experimentally.[7–11] These developments have inspired concepts for new kinds of spintronic devices and applications.[12,13]

Driven by curiosity and encouraged by the potential for applications, researchers have also started to investigate heterostructures involving high-T_c cuprate superconductors (HTSC) and ferromagnetic manganites.[14–19] The common perovskite-related structure and similar in-plane lattice parameters, together with recent improvements in film deposition techniques, enable the layer by layer controlled epitaxial growth of multilayers and superlattices (SLs) with very sharp interfaces.[17,20] Experiments on this kind of oxide SC/FM heterostructures revealed effects such as a change in the SC critical temperature T_c related to the presence and thickness of the FM layers, and vice versa;[17,19] a SC-related giant

magnetoresistance in FM/SC/FM trilayers;[21] the enhancement of T_c by an external magnetic field;[22,23] and even a SC-induced modulation of the magnetic moment in the FM layers.[24] These observations provide encouraging evidence for a sizable interaction between the SC and FM order parameters in these cuprate/manganite multilayer systems. They also show that not only the superconducting but also the magnetic properties of these oxide heterostructures are extremely versatile and need to be thoroughly investigated.

Polarized neutron reflectometry (PNR) measurements on YBa$_2$Cu$_3$O$_7$/La$_{2/3}$Ca$_{1/3}$MnO$_3$ (YBCO/LCMO) SLs have indeed revealed an unusual kind of magnetic proximity effect that gives rise to a significant change of the FM order in the vicinity of the YBCO/LCMO interfaces. PNR measurements on SLs with equally thick YBCO and LCMO layers, for which the even-order superlattice Bragg peaks should be absent for symmetry reasons, showed that a second-order Bragg peak appears and gains considerable intensity below the FM transition temperature T^{Curie} of the LCMO layers.[25] This observation clearly showed that the depth profile of the magnetic potential has a lower local symmetry than the nuclear one. In other words, the FM moment is either significantly modified (reduced) on the LCMO side of the interface or a FM moment is induced on the YBCO side. Two different models were proposed in Ref. 25 to describe this magnetic proximity effect: a so-called "dead layer model" with a strongly reduced

magnetization on the LCMO side, and a so-called "inverse proximity effect model" where ferromagnetic Cu moments antiparallel to the Mn moments in LCMO are induced on the YBCO side of the interface. It was not possible to distinguish between these two possibilities since the PNR data contained only a fairly limited range in momentum space such that the superlattice Bragg peaks beyond the second order were not observed. Later on, it was found that this is due to a problem of the SrTiO$_3$ (STO) substrates for which a structural transition below 100 K can give rise to a buckling of the surface with micrometer-sized structural domains that are tilted up to 0.5°.[24,26] It was shown that this tilting extends into the SL on top of the STO substrate and thus gives rise to a large broadening or even a pronounced splitting of the PNR specular signal along the 2θ direction of the detector.

In the meantime, i.e., before this problem with the STO substrates had been fully appreciated, additional experiments of YBCO/LCMO SLs on STO substrates were reported that supported either the dead layer model or the inverse proximity effect model. Hoffmann *et al.* reported an enhancement in the Mn 3*d* occupation next to the interface and concluded that their PNR data support the dead layer model.[27] On the other hand, Chakhalian *et al.* reported x-ray magnetic circular dichroism (XMCD) data which established the presence of a ferromagnetic Cu moment and thus were interpreted in terms of the "inverse proximity effect model."[28] Seemingly contradictory results were also reported concerning theoretical calculations. The density functional theory calculations performed by Luo *et al.* predicted a strongly reduced ferromagnetic or even antiferromagnetic coupling for the Mn atoms next to the interfaces,[29] whereas the theoretical work of Salafranca *et al.* concluded that the negative spin polarization of Cu in YBCO layers is a key ingredient to explain the observed enhancement of T_c with magnetic field observed in LCMO/YBCO/LCMO trilayers.[22,30]

More recently, some of the present authors have been shedding new light on this seemingly contradictory issue of the magnetic proximity effect. They investigated a YBCO/LCMO SL on a La$_{0.3}$Sr$_{0.7}$Al$_{0.65}$Ta$_{0.35}$O$_3$ (LSAT) substrate which is well lattice-matched and avoids the complications of the buckling of the STO substrates.[31] On this SL they performed a combination of PNR, XMCD, and x-ray resonant magnetic reflectometry (XRMR) which showed that the magnetic proximity effect at the YBCO/LCMO interface involves in fact both phenomena, i.e., a suppression of the FM moment on the LCMO side and, yet, an induced ferromagnetic Cu moment on the YBCO side. The latter was firmly established by the XMCD and especially by the XRMR measurements at the Cu-L edge which confirmed that the ferromagnetic Cu moments reside within the YBCO layers. Specifically, they demonstrated that the ferromagnetic Cu moments do not arise from a small amount of Cu ions that might have been incorporated in the LCMO layers. The existence of a layer with a depleted FM moment on the LCMO side was inferred from the analysis of the PNR data which extend with a sufficient signal-to-noise ratio to the fourth-order superlattice Bragg peak. In this manuscript we present the details of the analysis of these PNR data which could not be shown in the previous short Letter. Specifically, we show that the "dead layer model," or rather the "depleted layer model" as we prefer to

call it for the reasons given below, accounts well for the PNR data. We also show that alternative models fail to reproduce important features of the PNR curves.

We remark that this observation has important implications. In combination with the XMCD and XRMR data, which reveal the existence of an induced FM Cu moment on the YBCO side of the interface, it suggests that a strongly reduced but finite FM order or possibly even a noncollinear magnetic order of the Mn moments persists in the depleted layer which mediates the antiparallel coupling between the Cu moments in YBCO and the Mn moments in the central part of the LCMO layers. The so-called depleted layer therefore should not be considered as a magnetically "dead layer;" instead it seems very much alive and may play an important role, for example, in the recently reported long-range SC proximity effect.[32,33]

I. EXPERIMENTAL

All the measurements presented in this report have been performed on the same [YBCO (10 nm) /LCMO (9 nm)]$_{10}$ SL that was grown on a LSAT substrate with pulsed laser deposition (PLD) as described elsewhere.[20] The substrate with a size of 10×10 mm^2 and a thickness of 0.5 mm was purchased from Crystec. The monolayer by monolayer growth has been controlled with *in situ* reflection high-energy electron diffraction (RHEED). Resistivity measurements were performed using the four-point probe option of a physical properties measurement system (PPMS) from Quantum Design (model QD6000). The magnetization was measured on a small piece cut from the corner of the sample using the vibrating sample magnetometer (model P525) option of the PPMS system. X-ray reflectivity (XRR) measurements were carried out with the UE56/2-PGM1 beamline at BESSY in Berlin, Germany, using the MPI-IS ErNST end station. The PNR measurements were performed with the two-axis reflectometers NREX at FRM-II in Munich, Germany, and SuperADAM at ILL in Grenoble, France. Magnetic fields up to 4 kOe oriented perpendicular to the scattering plane and parallel to the film surface were produced with electromagnets. The temperatures and applied magnetic fields were as follows: (4 K, 4000 Oe, NREX), (100 K, 4000 Oe, NREX), (300 K, 0 Oe, NREX), (10 K, 100 Oe, SuperADAM), (100 K, 100 Oe, SuperADAM), (300 K, 0 Oe, SuperADAM).

The PNR curves have been fitted using the SUPERFIT package originally developed at the Max-Planck-Institut Stuttgart.[34] This package uses the maximum likelihood probability algorithm to define the minimizing function; the minimization is performed with the MINUIT package.[35] The likelihood estimator is defined as

$$l = \sum_{i=1}^{N} \left[y_i - x_i + x_i \ln\left(\frac{x_i}{y_i}\right) \right],$$

where N is the total number of data points, x_i is the measured intensity, and y_i is the calculated intensity using the supermatrix formalism.[36] Reported in the following is the reduced likelihood estimator $l^{\text{red}} = l/(N - n)$, where n is the number of fitted parameters. We used a modified version of the SUPERFIT program, which allows us to fit several data sets simultaneously with global parameters, to fit more reliably the

common structural parameters. The simulations of the XRR data have been performed using the software package GenX.[37]

II. RESULTS AND DISCUSSION

Figure 1 shows the temperature dependence of the resistance and the field-cooled (FC) magnetization of the YBCO/LCMO SL. The resistance shows a sharp decrease at the onset of the superconducting transition at $T_c = 88$ K and vanishes below 72 K. The ferromagnetic transition at $T^{\text{Curie}} = 201$ K is evident from the sudden increase in the magnetic moment as well as from a kink in the temperature dependence of the normal state resistance. The latter feature originates from the insulator-to-metal transition in the LCMO layer which coincides with the ferromagnetic ordering.

Figure 2 shows the unpolarized neutron reflectivity curves that were obtained at room temperature. The slight differences between the two curves are due to the different experimental configurations; for SuperADAM we used a high-resolution setup whereas for NREX the signal-to-noise ratio was enhanced at the expense of a lower resolution. Both curves exhibit a sharp reflection edge and a set of well-defined superlattice Bragg peaks (SLBPs). The latter originate from the constructive interference between the neutron waves that are reflected from all the interfaces of the SL. The position, width, and intensity of the SLBPs contain the information about the average value and the variation of the thickness of the individual YBCO and LCMO layers. Additional information about the roughness of the SL is contained in the form of the overall decrease toward large momentum transfer of the reflectivity curve beyond the reflection edge. In the absence of roughness this decrease follows a q_z^{-4} law, where q_z is the value of the normal momentum transfer. The roughness makes this overall decrease of the intensity of the reflectivity curve even faster.

The high-resolution data from SuperADAM also show a high-frequency oscillation in the q_z range between the reflection edge and the first SLBP. These are so-called Kiessig fringes that originate from the interference between the reflections from the surface (ambient/LCMO) and the bottom
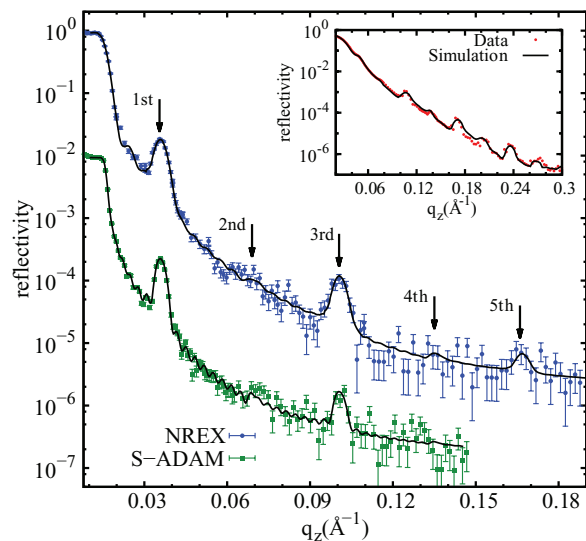
FIG. 2. (Color online) Unpolarized neutron reflectivity curves of the YBCO/LCMO SL measured at room temperature with the NREX and SuperADAM instruments. The curves are vertically shifted for clarity. Symbols show the experimental data and solid lines the best fits that were obtained by fitting both curves simultaneously. The arrows mark the position of the SLBPs. Inset: Symbols show the nonresonant XRR curve at 300 K. The solid line shows a simulation using the parameters as obtained from the fits of the neutron reflectometry curves.

(interface with the LSAT substrate) of the SL. These features testify to the high quality of our SL; from their period we can deduce the thickness of the entire SL. The thickness of the YBCO/LCMO bilayers can be inferred from the position of the SLBPs. The information about the thickness ratio of the YBCO and LCMO layers is contained in the intensity variation of the even- and odd-order SLBPs. For example, the even-order SLBPs are entirely suppressed if the YBCO and LCMO layers have exactly the same thickness. This is a destructive interference phenomenon that originates from a π-phase shift between the neutron waves that are reflected at the YBCO/LCMO and the LCMO/YBCO interfaces. It arises because the scattering potential exhibits a steplike increase at one of the interfaces and a corresponding decrease on the opposite one. In the reflectivity curves in Fig. 2 the intensity of the second- and fourth-order SLBPs is indeed much weaker than the one of the first- and third-order SLBPs. The finding that the suppression of the even-order SLBP intensity is not complete, i.e., that a small increase is observed at the position of the second- and the fourth-order SLBPs, shows that there is a small mismatch between the thicknesses of the YBCO and LCMO layers.

As a starting point of our analysis we have simultaneously fitted the two room-temperature unpolarized neutron reflectivity curves to extract the structural parameters. The result of the best fit is shown by the solid lines in Fig. 2 and can be seen to describe the experimental data (symbols) very well. The obtained values of the nuclear scattering length density (SLD) are $\rho_{\text{YBCO}}^{N} = 4.511(12) \times 10^{14}$ m^{-2} and $\rho_{\text{LCMO}}^{N} = 3.531(12) \times 10^{14}$ m^{-2}; the thickness parameters are $d_{\text{YBCO}} = 9.773(72)$ nm and $d_{\text{LCMO}} = 9.087(72)$ nm. The latter
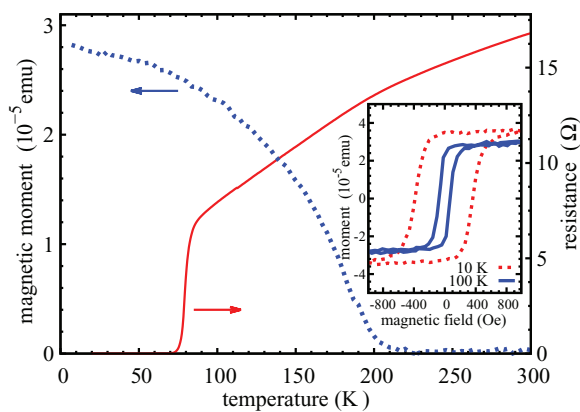

FIG. 1. (Color online) Temperature dependence of the resistance and the magnetic moment in field-cooled (FC) mode with $H = 100$ Oe applied parallel to the layers as measured on the YBCO/LCMO superlattice. It shows the onset of the superconducting transition at $T_c = 88$ K and the ferromagnetic transition at $T^{\text{Curie}} = 201$ K. Inset: Magnetic hysteresis loops measured at 10 K and 100 K.
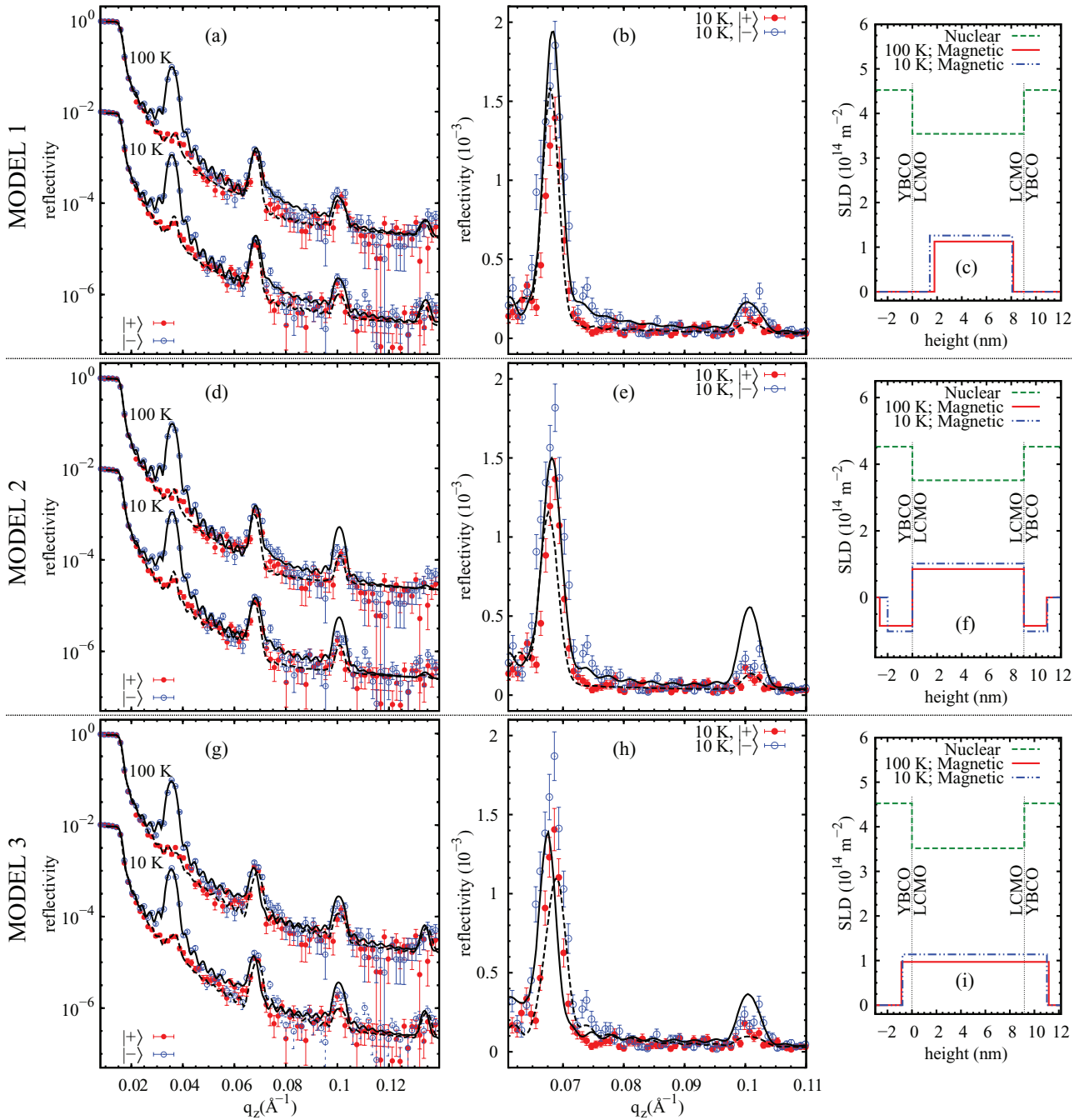
FIG. 3. (Color online) (a) Polarized neutron reflectivity curves of the YBCO/LCMO SL measured at low temperature after field cooling in 100 Oe at SuperADAM for up $|+\rangle$ and down $|-\rangle$ polarization of the neutron spin with respect to the direction of the applied magnetic field. The lines show the best fit for the depleted layer model for $|+\rangle$ (dashed) and $|-\rangle$ (solid) neutron spin channels. For clarity the curves at 10 K are vertically shifted down by a factor of 10^2. (b) Close-up on a linear intensity scale in the region of the second and third SLBPs to aid the comparison with the fit. The depth profiles of the used nuclear and magnetic scattering length densities are shown in (c). The same data are shown in (d)–(f) together with the best fit using the model of an inverse magnetic proximity effect and, in (g)–(i), for the model of an induced FM moment in YBCO that is parallel to the one in LCMO.

correspond to approximately 8 and 23 unit cells per YBCO and LCMO layer, respectively. The obtained average interface roughness of 8.5(2) Å is within experimental resolution the same for both the YBCO/LCMO and LCMO/YBCO interfaces. This value is slightly smaller than the *c*-axis parameter of the YBCO unit cell and thus testifies to the high quality of the SL. As a consistency check, we have used

the obtained parameters for the thickness and roughness to simulate the XRR curve that was measured on the same SL. The inset of Fig. 2 shows the good agreement between the experimental curve (symbols) and the calculation (solid lines) for which only the value of the SLD has been adjusted.

Figures 3 and 4 show the low-temperature PNR curves which have been measured after field cooling in magnetic
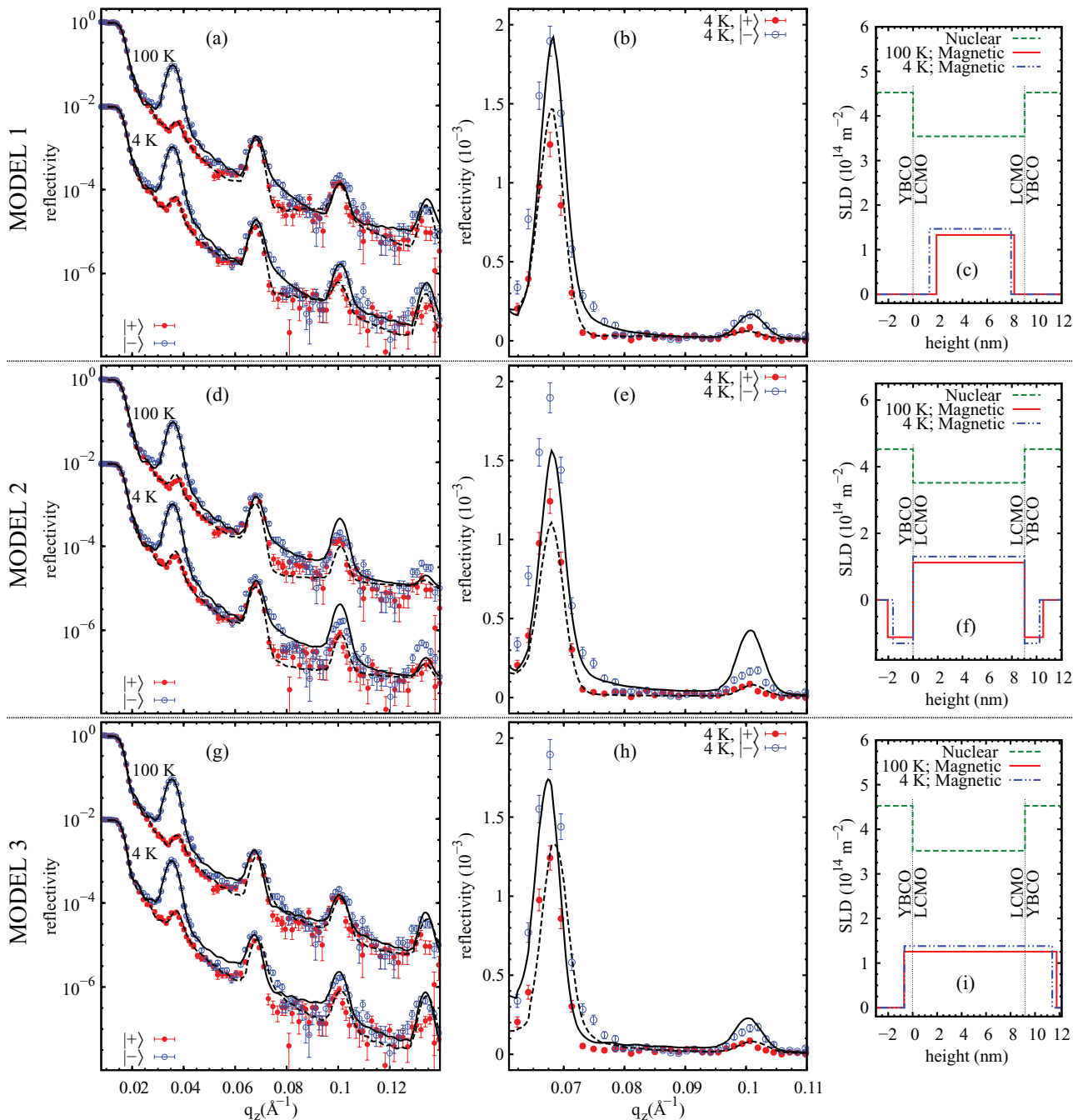
FIG. 4. (Color online) Same as in Fig. 3 but for the PNR data measured at NREX with an applied field of 4 kOe.

fields of 100 Oe and 4 kOe with SuperADAM and NREX, respectively. The magnetization loops in Fig. 1 show that at 4 kOe the sample is already fully magnetized. At 100 Oe the sample is not fully saturated; the field-cooled magnetization data in Fig. 8 show that the magnetization reaches about 80% of the saturation value. In fitting these PNR curves the structural parameters as obtained from the room-temperature curves (as described above) have been used as a constraint that can vary only within the error bar. This seems well justified, since the expected changes due to the temperature dependence of the lattice parameters of YBCO and LCMO are well within these error bars. We have also confirmed with temperature-dependent x-ray measurements on a LSAT substrate that it

does not undergo any anomalous structural change. In addition, Fig. 5 shows the off-specular scattering at 300 and 4 K which confirms that the anomalous broadening and splitting of the specular reflection curves that was previously reported for similar SLs on STO substrates at temperatures below 100 K[24,26,38] is absent for the present YBCO/LCMO SL on LSAT. The comparison of the maps in Figs. 5(a) and 5(b) shows that for the reflection edge and the SLBPs the width in the off-specular direction is small and does not change significantly between 300 and 4 K. The quality of the specular reflectivity curves at low temperature accordingly remains very high. As shown in Figs. 3 and 4, the intensity of the reflectivity curves does not fall off significantly faster at 10 K or 4 K than
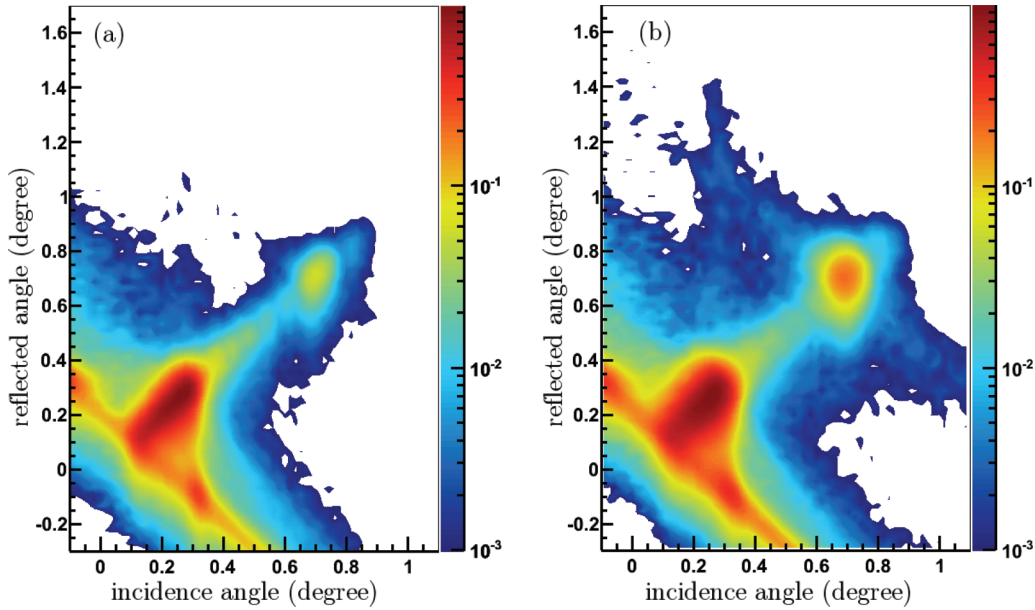
FIG. 5. (Color online) Maps of the off-specular reflection of the YBCO/LCMO superlattice measured (a) with unpolarized neutrons at 300 K and (b) for the $|+\rangle$ spin channel at 4 K after field cooling in a field of 100 Oe.

at 300 K and the signal remains well above the background level for the q_z values up to 0.14 Å^{-1} which includes the fourth-order SLBP.

The shape of the reflectivity curves below $T^{\text{Curie}} = 201$ K, as shown in Figs. 3 and 4, depends on whether the incident neutron spin is parallel ($|+\rangle$) or antiparallel ($|-\rangle$) to the applied magnetic field. This is due to the additional magnetic potential which is comparable in size to the nuclear one and for which the sign depends on the orientation of the FM moments with respect to the one of the neutron spins. It is also evident that the second- and the fourth-order SLBPs, which were almost absent in the curves at 300 K, have gained a lot of intensity and became very pronounced features in the PNR curves at 100 K, 10 K, and 4 K. As was already discussed in the introduction, this is a clear indication that the magnetic potential has a lower local symmetry than the nuclear one. For the latter the even-order SLBPs were almost absent due to the similar thickness of the YBCO and LCMO layers. The magnetic potential due to the ferromagnetic order obviously does not exhibit a steplike increase right at the YBCO/LCMO interface or a corresponding decrease at the LCMO/YBCO interfaces. Instead, there must be either a significant decrease of the FM moment on the LCMO side of the interface or a corresponding increase on the YBCO side.

Due to the lack of the phase information in the reflectometry measurement the shape of the depth profile of the magnetic potential cannot be directly extracted from the PNR data. The reflectivity curves can still be analyzed with different realistic models and their validity can be judged based on how well they reproduce the data. As was the case in Ref. 25, it may still happen that different models lead to similar results and therefore cannot be distinguished. In the following we show that this ambiguity can be overcome with reflectivity curves that extend up to larger q_z values where the differences between the various models become more pronounced.

We consider three different models and evaluate how well they can reproduce the PNR data. Model 1 corresponds to the depleted layer model that has been outlined in the introduction. For simplicity, a layer with a completely suppressed FM moment is introduced here on the LCMO side of each interface. The thickness of this layer is a fitting parameter.

Model 2 describes the inverse magnetic proximity effect, where FM moments antiparallel to the Mn moments in LCMO are induced on the YBCO side of the interface. In the first place, one expects that these are the Cu moments which have been observed with the XMCD and XRMR measurements. However, the magnitude of these ferromagnetic Cu moments is reported to be only ∼0.25 μ_B.[31] Therefore, it remains to be seen whether they can account for the observed large increase of the intensity of the even-order Bragg peaks. On the other hand, we cannot completely exclude the possibility that an additional, possibly even larger contribution arises from some Mn ions that may have been incorporated in the YBCO layers, for example due to an unwanted contamination or a diffusion across the interface during the growth.

Model 3 accounts for a similar case where the induced FM moment on the YBCO side is parallel to the one of the Mn moments in LCMO and to the applied magnetic field. Such a contribution would have to arise solely from the Mn moments, since the XMCD and XRMR data clearly established the antiparallel orientation of the Cu moments.

For all three models we had to use a modified magnetic potential for the topmost LCMO layer; i.e., a 2–3 nm thick nonmagnetic layer has been introduced at the film surface. This was necessary to reproduce the sizable differences between the $|+\rangle$ and $|-\rangle$ curves in the region right before and after the first-order SLBP. We suspect that this effect arises from the interaction of the surface layer with the ambient which degrades the FM order in the first few LCMO monolayers.

In the following we use the quality of the best fits as the criterion to determine the validity of each model. In addition,

we compare the average value of the magnetization obtained from the model with the experimental result as measured with dc magnetization.

Figures 3 and 4 show the PNR curves at 100 K, 10 K, and 4 K with the best fits for each model (solid and dashed lines) together with the obtained depth profiles of the nuclear and magnetic scattering length densities. As was already mentioned, the structural parameters have been constrained to lie within the error bars of the parameters derived from the unpolarized room-temperature curves. The obtained reduced likelihood estimators for models 1, 2, and 3 of $l_1^{\text{red}} = 4.12$, $l_2^{\text{red}} = 5.18$, and $l_3^{\text{red}} = 7.37$, respectively, are in favor of model 1. The specific features where models 2 and 3 fail to describe the experimental data are discussed next.

The close-up in Figs. 3(h) and 4(h) reveals that model 3 predicts a shift in the position of the second-order SLBP towards lower (higher) q_z for the $|-\rangle$ ($|+\rangle$) curve. Such a shift is not observed in the experimental data where the maxima nearly coincide and the splitting of the curves is due to the different intensities of the peaks. The disagreement is especially obvious on the high-q_z side of the second-order SLBP where the intensity of the fitted $|+\rangle$ curve is higher than for the corresponding $|-\rangle$ curve, whereas in the experimental data the opposite trend is observed. Such a discrepancy was already noted in Ref. 25 and was used to discard model 3. Furthermore, we note that a rather large value of the induced magnetization in the YBCO layers has to be assumed for model 3 to account for the large intensity of the second-order SLBP. For the fits in Figs. 3 and 4 the FM moment in the YBCO layer has been constrained to have the same value as the one in the LCMO layers. When it was released, the induced magnetization reached even larger values whereas the quality of the fit was not significantly improved. Already the constrained value appears to be unreasonably large; e.g., for the PNR curves taken at 4 kOe it reaches $\sim 2.7 \mu_{\text{B}}$. Such a large ferromagnetic moment on the YBCO side of the interface cannot arise from the induced Cu moments; it would also require an unrealistically large concentration of Mn ions.

Model 2, as shown in the close-ups in Figs. 3(e) and 4(e), can account reasonably well for the data in the vicinity of the second-order SLBP. Nevertheless, it largely overestimates the intensity of the third-order SLBP in the $|-\rangle$ curve. The intensity of the third-order SLBP in the simulation could be reduced assuming an increased roughness of the magnetic potential. However, this would lead to a faster decay of the curve to the background level which is not observed. It would also further enhance the discrepancy at the fourth-order SLBP where the fit already severely underestimates the peak intensity of the $|-\rangle$ curve. Furthermore, model 2 has the same problem as model 3 concerning the very large value of the induced moment in the YBCO layers that has to be assumed. Once more, for the fit in Figs. 3(d) and 4(d) the FM moment in the YBCO layer has been constrained to be the same as the one in the LCMO layers; i.e., at 4 kOe it reaches $\sim 2.7 \mu_{\text{B}}$. This value is larger than the moment of $\sim 1 \mu_{\text{B}}$ of Cu^{+2} and one order of magnitude larger than the value reported from the XMCD measurements performed on the same sample, $\sim 0.25 \mu_{\text{B}}$.[31] If the induced magnetic moment is for example bounded to $1 \mu_{\text{B}}$, the intensity of the second-order SLBP is largely reduced and the overall quality of the fit is

strongly reduced. Model 1 is clearly the one that reproduces the measured data the best and yields a realistic magnitude of the ferromagnetic moments. The position, spin splitting, and intensity of all SLBPs are reasonably well described. Only the overestimation of the intensity of the fourth-order SLBP in the $|+\rangle$ curve at NREX can be regarded as a significant mismatch between the simulation and the data. The very fact that such a simple blocklike model reproduces all features of the measurement is remarkable and confirms that it contains the main characteristics of the magnetic depth profile of the SL. These simulations clearly establish the trend that a sizable suppression of the FM moment on the LCMO side of the interface is responsible for the occurrence of the even-order SLBPs. The characteristic length of the decay of the ferromagnetic moment at the interface should therefore be directly related to the calculated thickness of the depleted layers which are shown in Table I for the different temperatures and fields.

For the bottom interface the depleted layer thickness is as large as 19 Å showing that the suppression of the magnetization extends rather far into the LCMO layers. The similar values of the thickness of the depleted layer (within the error bars) at 100 Oe and 4 kOe show that the depleted layer is hardly affected by the external magnetic field. This excludes for example an explanation in terms of a different ferromagnetic phase that has a larger saturation field than the one in the center of the LCMO layers. It also appears that the thickness of the depleted layer is consistently larger for the bottom interface than for the one on top of the LCMO layer (in terms of the SL growth direction). The origin of this difference is not known. It may be related to a structural difference that is imposed by a different growth process. However, as already discussed, concerning the roughness we did not find a significant difference between the top and bottom interfaces. Furthermore, a recent transmission electron microscopy (TEM) study on superlattices that were grown under identical conditions did not provide any indication for such a difference.[20] Surprisingly, but in good agreement with a previous study of similar superlattices on STO substrates,[39] the TEM images reveal that both the YBCO/LCMO and the LCMO/YBCO interfaces involve the same kind of CuO$_2$-Y-CuO$_2$-BaO-MnO$_2$ layer stacking sequence for which the last YBCO unit cell is lacking the CuO chains. The expected asymmetry of the interfaces, where a CuO chain layer should be adjacent to one of the interfaces and a CuO$_2$ bilayer to the other one, could not be observed. This still leaves the possibility that the layer separating the CuO$_2$ and MnO$_2$ planes may have a different stoichiometry; i.e., it may have a variable Ba and La or Ca content. At the lowest temperatures of 4 K

TABLE I. Thickness of the depleted layers at the bottom and top interfaces as obtained with model 1 at different temperatures and applied magnetic fields.

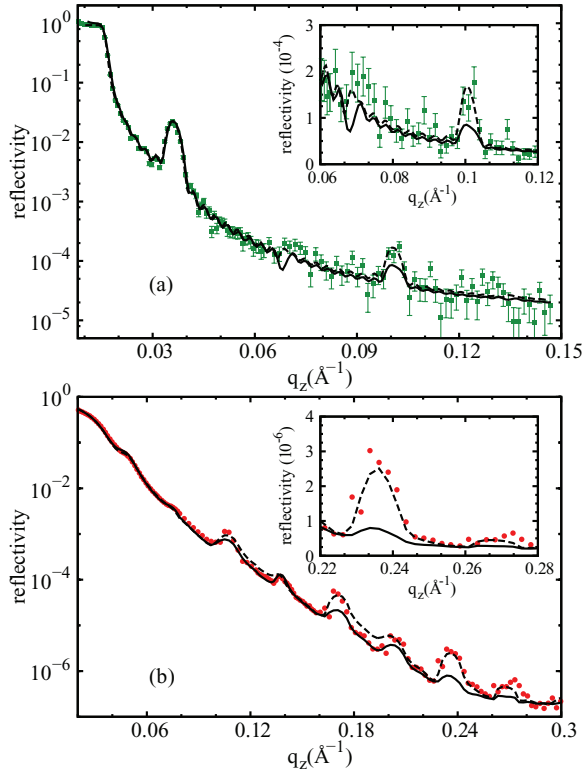| T, H	$d_{\text{dep}}^{\text{bottom}}$ (Å)	$d_{\text{dep}}^{\text{top}}$ (Å)
10 K, 100 Oe	14.0(7)	9.3(7)
100 K, 100 Oe	17.9(7)	8.5(7)
4 K, 4 kOe	13.2(7)	11.0(7)
100 K, 4 kOe	19.0(7)	8.4(7)

FIG. 6. (Color online) Room-temperature reflectivity curves (symbols) of the YBCO/LCMO SL measured with (a) neutrons and (b) x rays. The dashed lines show the best fit with a roughness of 8.5 Å at both the top and bottom interfaces that was also shown in Fig. 2. The solid lines show a simulation in which a roughness of 16 Å and 9.5 Å was assumed for the LCMO bottom and top interfaces, respectively. Insets: Magnification around the high-order SLBPs to highlight the difference between the two models.

and 10 K, the thickness of the bottom (top) depleted layers is reduced (increased) with respect to the values at 100 K. These changes lead to a sizable reduction of the asymmetry between the two interfaces.

We emphasize that the depleted layers cannot be simply interpreted in terms of a roughness-induced effect. While the average thickness of the top depleted layers ($\sim$9.5 Å) and the interface roughness that is obtained from the room-temperature PNR and XRR curves ($\sim$8.5 Å) are similar, the large thickness of the depleted layer at the bottom interface (up to 19 Å) suggests that there is no correlation between the size of the depleted layers and the interface roughness. Figure 6 shows that both the PNR and the XRR data are not in agreement with a model for which the interface roughness is assumed to match the average thickness of the depleted layers of 16 Å and 9.5 Å for the bottom and top LCMO interfaces, respectively. There is a clear trend that such an enhanced interface roughness would lead to a stronger suppression of the intensity of the higher order SLBPs than is observed in the experiment. It would also yield the wrong size and shape of the symmetry-forbidden second-order SLBP. Besides, such a structural roughness could also not explain the observation that the thickness of the depleted layer exhibits a significant temperature dependence as discussed above.
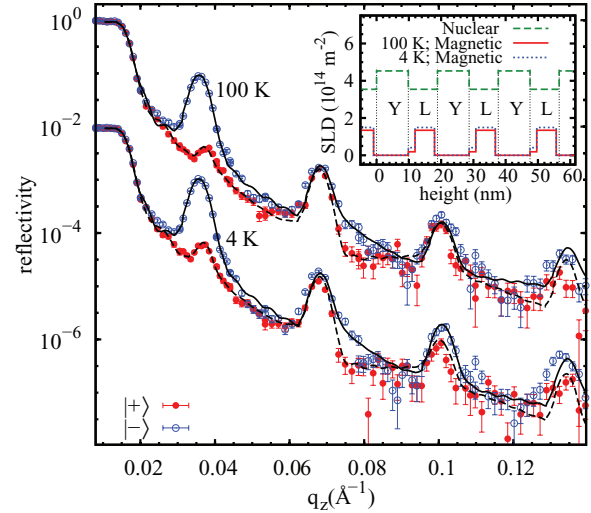

FIG. 7. (Color online) Low-temperature PNR curves of the YBCO/LCMO SL at 4 kOe. The solid and dashed lines are the results of the fit using model 1a; here the magnetization in the depleted layers is fitted and the thicknesses of the top and bottom interfaces are set as common among all data sets.

To obtain further information about the magnetic nature of the depleted layers, we have modified the fitting with model 1 by allowing for a finite magnitude of the FM moments in the depleted layer (treating the net magnetization in the depleted layers as a fitting parameter). To keep the number of fitting parameters reasonably low, we have now set the thickness of the depleted layers for the top and bottom interfaces to be common for all temperatures and fields. This modification is labeled as model 1a and the comparison of the fitted curves using this model and the PNR data at 4 kOe data is shown in Fig. 7. The inset shows the obtained depth profile of the scattering length densities, for which the magnetic part is proportional to the FM moment. In agreement with the results obtained for model 1, shown in Table I, the thicknesses of the top and bottom depleted layers are calculated as 9.2(7) Å and 20.1(7) Å, respectively. It appears that the best fit obtained with model 1a is indeed very similar to the one of model 1 (see Fig. 4) and results in the same value of the reduced likelihood estimator of $l_{1a}^{red} = 4.12$. The fit with model 1a yields a finite magnetic scattering length density near the bottom interface corresponding to a FM moment of about 20% of the one in the central part of the LCMO layers. This value increases slightly as the temperature is reduced from 100 K to 4 K, in good agreement with model 1 where a corresponding decrease of the depleted layer thickness was obtained. Near the top interface the fit with model 1a does not yield a finite value of the FM moment. Nevertheless, given the crude assumption of blocklike magnetic potentials, we are not sure whether these fit results are significant. Therefore we cannot draw any firm conclusion about the presence of a small ferromagnetic moment in the depleted layers.

As a next step, we have addressed the question of whether the induced ferromagnetic Cu moments in the YBCO layers are playing a significant role for the fitting of the PNR curves. The presence of these Cu moments was confirmed by the XMCD and XRMR measurements performed on the same

sample which suggest an average FM moment of 0.25 μ_B per Cu ion that is antiparallel to the applied field and the moments in LCMO.[31] We have therefore modified model 1 to allow in addition to the depleted layers on the LCMO side for a small, antiparallel moment on the YBCO side. It turned out that these Cu moments do not significantly modify or improve the fit results. This is not surprising since these Cu moments are about ten times smaller than the Mn moments in the central part of the LCMO layers and so are the corresponding values of the magnetic potential and the magnetic scattering length density. The PNR curves thus are governed by the larger magnetic moments inside the LCMO layers and are hardly sensitive to the much smaller Cu moment in the YBCO layers. While the PNR technique apparently is not sensitive to these ferromagnetic Cu moments, we point out once more that these have been unambiguously identified with resonant x-ray absorption and reflection techniques.[28,31]

Finally, we have tested the validity of the fits as obtained with models 1–3 by comparing the average magnetic moment of the fitted profile [see Figs. 3 and 4, panels (c), (f), and (i)] with the experimental value as obtained from dc magnetization measurements. The result is summarized in Fig. 8 which shows the magnetic moment from the field-cooled dc magnetization measurements at 100 Oe and 4 kOe (solid lines) together with the magnetic moments as calculated from the best fits of models 1, 1a, 2, and 3 to the PNR curves at 100 Oe and 4 kOe (symbols). This comparison shows a very good agreement for models 1 and 1a and large discrepancies for models 2 and 3. For model 3 where the FM moments in the LCMO and YBCO layers are assumed to be parallel, the calculated magnetic moment is almost twice as large as the
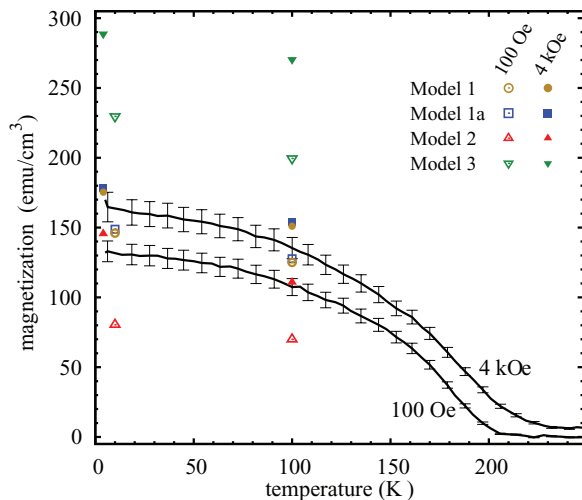

FIG. 8. (Color online) Comparison of the average magnetic moment as determined experimentally from field-cooled dc magnetization measurements at 100 Oe and 4 kOe (solid lines) and calculated from the magnetic potential obtained with model 1 (circles), model 1a (squares), model 2 (upwards triangles), and model 3 (downwards triangles) from the fits to the PNR curves measured at 100 Oe (open symbols) and 4 kOe (solid symbols). The size of the symbols of the calculated magnetic moments reflects the error bars. The error bars of the dc magnetization data arise from the statistical errors and the uncertainty of the volume of the small piece used for the dc magnetization measurements.

measured one. For model 2 the calculated magnetic moments are significantly smaller than the measured ones. Evidently, this is a consequence of the assumption that the FM moment in the YBCO layers is antiparallel to the ones in the LCMO layers. This comparison clearly argues against models 2 and 3 and emphasizes the relevance of models 1 and 1a in terms of the depleted FM layer on the LCMO side of the interfaces. The discrepancy between the calculated magnetic moment of models 1 and 1a and the experimentally measured value never exceeds 15% and it is almost within the error bars. Given the simplicity of the model, with its simple blocklike potentials, this agreement can be considered as excellent. The somewhat larger difference that appears in the low-field data at 100 Oe, where the magnetization is not yet fully saturated, may have its origin in a weak spin-flip scattering which would contribute to both spin channels, especially around the first Bragg peak, and thus enhance the calculated magnetic moment.

To conclude, the analysis of the PNR data as shown above provides clear evidence for the presence of a so-called depleted layer on the LCMO side of the interfaces in which the ferromagnetic moment of the Mn ions is strongly suppressed as compared to the one in the central part of the LCMO layers. These depleted layers extend into the LCMO layers up to distances larger than the calculated interface roughness and therefore are not likely just the result of chemical and/or structural disorder. At the top interface the depleted layer extends over about 3 LCMO unit cells (with a lattice parameter of 3.9 Å) and at the bottom interface it involves even 4–5 LCMO unit cells. The depleted layer thickness also has a significant temperature dependence. When cooling from 100 K to 10 K or 4 K, the asymmetry between the interfaces is reduced and the total thickness of the depleted region decreases considerably. As reported in Ref. 31, this decrease appears to be even anomalously enhanced below the superconducting transition temperature. Additional evidence for an intrinsic electronic origin of the depleted layers in the YBCO/LCMO SL comes from the observation that the magnetic proximity effect and thus these depleted layers are absent for a corresponding YBCO/LaMnO$_{3+\delta}$ SL for which the manganite layers are insulating.[31] The large FM moments of the Mn ions persist here right up to the interface. Furthermore, there is the observation of the XMCD and XRMR studies that a ferromagnetic (or strongly canted antiferromagnetic) order of the Cu moments is induced on the YBCO side of the interfaces of the YBCO/LCMO SL. Notably, these Cu moments are much weaker or even absent in the YBCO/LMO SLs where the FM order of the Mn moments persists right up to the interface. These observations suggest that the induced ferromagnetic Cu moments in the YBCO layers are a central part of the magnetic proximity effect just as much as the suppression of the FM moment on the LCMO side of the interface. The apparent antiparallel coupling between the induced Cu moments in the YBCO layers and the Mn moments therefore requires that the depleted layer maintain some kind of magnetic order. Likely, this involves a noncollinear magnetic order that cannot be detected with the PNR technique which probes the average FM component.

We note that such a noncollinear magnetic order may have important consequences for the superconducting proximity effect in these YBCO/LCMO superlattices. It was previously shown that it can induce a spin-triplet component of the

superconducting order parameter which has a long-ranged proximity effect into the FM layers.[3,12] Evidence for such a scenario has indeed been reported very recently based on the observation of equal-spin Andreev reflections in YBCO/LCMO interfaces.[32]

III. SUMMARY

We have performed wide q_z range PNR measurements in a YBCO/LCMO SL for different applied fields and temperatures. The emergence of the second-order SLBP below T^{Curie} evidences a mismatch of the magnetic potential with respect to the nuclear one. After fitting the data with three different models and comparing the results we have ruled out the possibility of an induced magnetic moment in YBCO as the main origin of the asymmetry. Our results suggest that the asymmetry in the potential mainly comes from the existence a so-called depleted layer in the LCMO side of the interface where the net FM moment is strongly reduced. The characteristic length of this reduction is larger than the expected interface roughness suggesting an electronic rather than structural origin for the depletion zones. The actual magnetic state of the depleted layers could consist of some canted or oscillatory order as suggested by the induction of a Cu moment in the YBCO side and the observation of long-range spin-triplet correlations inside the FM layers in a similar system.

*miguelangel.uribelaverde@unifr.ch

†Present address: Department of Physics, Indian Institute of Technology Madras, 600036 Chennai, India.

[1] L. Bulaevskii, A. Buzdin, M. Kuli, and S. Panjukov, Adv. Phys. **34**, 175 (1985).

[2] A. I. Buzdin, Rev. Mod. Phys. **77**, 935 (2005).

[3] F. S. Bergeret, A. F. Volkov, and K. B. Efetov, Rev. Mod. Phys. **77**, 1321 (2005).

[4] A. I. Buzdin and A. S. Mel'nikov, Phys. Rev. B **67**, 020503 (2003).

[5] J. Kehrle, V. Zdravkov, G. Obermeier, J. Garcia-Garcia, A. Ullrich, C. Müller, R. Morari, A. Sidorenko, S. Horn, L. Tagirov, and R. Tidecks, Ann. Phys. **524**, 37 (2012).

[6] A. F. Volkov, F. S. Bergeret, and K. B. Efetov, Phys. Rev. Lett. **90**, 117006 (2003).

[7] T. Kontos, M. Aprili, J. Lesueur, F. Genêt, B. Stephanidis, and R. Boursier, Phys. Rev. Lett. **89**, 137007 (2002).

[8] Y. Blum, A. Tsukernik, M. Karpovski, and A. Palevski, Phys. Rev. Lett. **89**, 187004 (2002).

[9] T. S. Khaire, M. A. Khasawneh, W. P. Pratt, and N. O. Birge, Phys. Rev. Lett. **104**, 137002 (2010).

[10] J. W. A. Robinson, J. D. S. Witt, and M. G. Blamire, Science **329**, 59 (2010).

[11] Z. Yang, M. Lange, A. Volodin, R. Szymczak, and V. V. Moshchalkov, Nat. Mater. **3**, 793 (2004).

[12] M. Eschrig, Phys. Today **64**(1), 43 (2011).

[13] N. G. Pugach and A. I. Buzdin, Appl. Phys. Lett. **101**, 242602 (2012).

[14] P. Przyslupski, S. Kolesnik, E. Dynowska, T. Skoskiewicz, and M. Sawicki, IEEE T. Appl. Supercond. **7**, 2192 (1997).

[15] A. Goldman, P. Kraus, K. Nikolaev, V. Vas'ko, A. Bhattacharya, and W. Cooley, J. Supercond. **14**, 283 (2001).

[16] H.-U. Habermeier, G. Cristiani, R. Kremer, O. Lebedev, and G. van Tendeloo, Physica C **364-365**, 298 (2001).

[17] Z. Sefrioui, D. Arias, V. Peña, J. E. Villegas, M. Varela, P. Prieto, C. León, J. L. Martinez, and J. Santamaria, Phys. Rev. B **67**, 214511 (2003).

[18] T. Holden, H.-U. Habermeier, G. Cristiani, A. Golnik, A. Boris, A. Pimenov, J. Humlíček, O. I. Lebedev, G. Van Tendeloo, B. Keimer, and C. Bernhard, Phys. Rev. B **69**, 064505 (2004).

[19] R. Werner, C. Raisch, A. Ruosi, B. A. Davidson, P. Nagel, M. Merz, S. Schuppler, M. Glaser, J. Fujii, T. Chassé, R. Kleiner, and D. Koelle, Phys. Rev. B **82**, 224509 (2010).

[20] V. K. Malik, I. Marozau, S. Das, B. Doggett, D. K. Satapathy, M. A. Uribe-Laverde, N. Biskup, M. Varela, C. W. Schneider, C. Marcelot, J. Stahn, and C. Bernhard, Phys. Rev. B **85**, 054514 (2012).

[21] V. Peña, Z. Sefrioui, D. Arias, C. Leon, J. Santamaria, J. L. Martinez, S. G. E. te Velthuis, and A. Hoffmann, Phys. Rev. Lett. **94**, 057002 (2005).

[22] N. M. Nemes, M. García-Hernández, S. G. E. te Velthuis, A. Hoffmann, C. Visani, J. Garcia-Barriocanal, V. Peña, D. Arias, Z. Sefrioui, C. Leon, and J. Santamaría, Phys. Rev. B **78**, 094515 (2008).

[23] K. Dybko, K. Werner-Malento, M. Sawicki, and P. Przyslupski, Europhys. Lett. **85**, 57010 (2009).

[24] J. Hoppler, J. Stahn, C. Niedermayer, V. K. Malik, H. Bouyanfif, A. J. Drew, M. Rossle, A. Buzdin, G. Cristiani, H.-U. Habermeier, B. Keimer, and C. Bernhard, Nat. Mater. **8**, 315 (2009).

[25] J. Stahn, J. Chakhalian, C. Niedermayer, J. Hoppler, T. Gutberlet, J. Voigt, F. Treubel, H.-U. Habermeier, G. Cristiani, B. Keimer, and C. Bernhard, Phys. Rev. B **71**, 140509 (2005).

[26] J. Hoppler, J. Stahn, H. Bouyanfif, V. K. Malik, B. D. Patterson, P. R. Willmott, G. Cristiani, H.-U. Habermeier, and C. Bernhard, Phys. Rev. B **78**, 134111 (2008).

[27] A. Hoffmann, S. G. E. te Velthuis, Z. Sefrioui, J. Santamaría, M. R. Fitzsimmons, S. Park, and M. Varela, Phys. Rev. B **72**, 140407 (2005).

[28] J. Chakhalian, J. W. Freeland, G. Srajer, J. Strempfer, G. Khaliullin, J. C. Cezar, T. Charlton, R. Dalgliesh, C. Bernhard, G. Cristiani, H.-U. Habermeier, and B. Keimer, Nat. Phys. **2**, 244 (2006).

[29] W. Luo, S. J. Pennycook, and S. T. Pantelides, Phys. Rev. Lett. **101**, 247204 (2008).

[30] J. Salafranca and S. Okamoto, Phys. Rev. Lett. **105**, 256804 (2010).

[31] D. K. Satapathy, M. A. Uribe-Laverde, I. Marozau, V. K. Malik, S. Das, Th. Wagner, C. Marcelot, J. Stahn, S. Brück, A. Rühm, S. Macke, T. Tietze, E. Goering, A. Frañó, J. H. Kim, M. Wu, E. Benckiser, B. Keimer, A. Devishvili, B. P. Toperverg, M. Merz, P. Nagel, S. Schuppler, and C. Bernhard, Phys. Rev. Lett. **108**, 197201 (2012).

[32] C. Visani, Z. Sefrioui, J. Tornos, C. Leon, J. Briatico, M. Bibes, A. Barthelemy, J. Santamaria, and J. E. Villegas, Nat. Phys. **8**, 539 (2012).

[33] T. Golod, A. Rydh, V. M. Krasnov, I. Marozau, M. A. Uribe-Laverde, D. K. Satapathy, Th. Wagner, and C. Bernhard, arXiv:1206.2053.

[34] SUPERFIT: Polarized Neutron Reflectivity Tool (Max Planck Institute for Intelligent Systems, Stuttgart).

[35] F. James and M. Roos, Comput. Phys. Commun. **10**, 343 (1975).

[36] A. Rühm, B. P. Toperverg, and H. Dosch, Phys. Rev. B **60**, 16073 (1999).

[37] M. Björck and G. Andersson, J. Appl. Crystallogr. **40**, 1174 (2007).

[38] J. Hoppler, H. Fritzsche, V. K. Malik, J. Stahn, G. Cristiani, H.-U. Habermeier, M. Rössle, J. Honolka, A. Enders, and C. Bernhard, Phys. Rev. B **82**, 174439 (2010).

[39] M. Varela, A. R. Lupini, S. J. Pennycook, Z. Sefrioui, and J. Santamaria, Solid-State Electron. **47**, 2245 (2003).